

A study of Si II and S II features in spectra of Type Ia supernova

Xulin Zhao^{1*}, Keiichi Maeda², Xiaofeng Wang³ and Hanna Sai³

¹*School of Science, Tianjin University of Technology, Tianjin, 300384, China*

²*Department of Astronomy, Kyoto University, Kitashirakawa-Oiwake-cho, Sakyo-ku, Kyoto 606-8502, Japan*

³*Physics Department and Tsinghua Center for Astrophysics, Tsinghua University, Beijing, 100084, China*

Accepted XXX. Received YYY; in original form ZZZ

ABSTRACT

We studied the spectral features of Si II $\lambda\lambda 4130, 5972, 6355$ and S II W-trough for a large sample of Type Ia supernovae (SNe Ia). We find that in NV (Normal-Velocity) subclass of SNe Ia, these features tend to reach a maximum line strength near maximum light, except for Si II $\lambda 5972$. Spectral features with higher excitation energy, such as S II W-trough, are relatively weak and have relatively low velocity. SNe Ia with larger $\Delta m_{15}(B)$ tend to have lower velocities especially at phases after maximum light. NV SNe show a trend of increasing line strength with increasing $\Delta m_{15}(B)$, while 91T/99aa-like SNe show an opposite trend. Near maximum light, the absorption depth of Si II $\lambda 5972$ shows the strongest correlation with $\Delta m_{15}(B)$, while at early times the sum of the depths of Si II $\lambda\lambda 4130$ and 5972 shows the strongest correlation with $\Delta m_{15}(B)$. The overall correlation between velocity and line strength is positive, but within NV SNe the correlation is negative or unrelated. In normal SNe Ia, the velocity-difference and depth-ratio of a longer-wavelength feature to a shorter-wavelength feature tend to increase with increasing $\Delta m_{15}(B)$. These results are mostly well explained with atomic physics, but some puzzles remain, possibly related to the effects of the saturation, line competition or other factors.

Key words: (stars:) supernova: general - methods: data analysis - techniques: spectroscopic

1 INTRODUCTION

Type Ia supernovae (SNe Ia) remain the best distance indicators on cosmological scales (Phillips 1993; Phillips et al. 1999; Riess et al. 1998, 2016, 2019; Perlmutter et al. 1999; Betoule et al. 2014; Dhawan et al. 2018; Jones et al. 2018; Scolnic et al. 2018; Freedman et al. 2019). However, their progenitor systems (e.g., Whelan & Iben 1973; Nomoto 1982; Nomoto et al. 1997; Iben & Tutukov 1984; Webbink 1984; Maoz et al. 2014; Cao et al. 2015; Olling et al. 2015; Maeda & Terada 2016; Blondin et al. 2017; Liu et al. 2018; Livio et al. 2018; Jha et al. 2019; Flörs et al. 2020) and the explosion mechanisms (Nomoto et al. 1984; Nomoto & Leung 2018; Khokhlov 1991; Hillebrandt & Niemeyer 2000; Maeda et al. 2010, 2018; Sim et al. 2012, 2013; Ruiter et al. 2013; Shen et al. 2014; Jha et al. 2019; Wu et al. 2020) remain unclear. Spectroscopic information is a key to unraveling the persistent mysteries. Many physical properties, such as the element distributions, the kinematics of the ejecta, the photospheric temperature, and the op-

tical depth can only be determined by spectroscopic methods (e.g., Sternberg et al. 2011; Dilday et al. 2012; Parrent et al. 2014; Maguire et al. 2018; Wilk et al. 2018; Jacobson-Galán et al., 2019).

SNe Ia spectra are characterized by strong absorption features of intermediate mass elements (IME) ions, such as Si II, S II and Ca II (see Filippenko et al. 1997, for a comprehensive review). Of particular interest is the prominent feature Si II $\lambda 6355$. The blueshifted velocity of the photospheric-velocity feature (PVF) of Si II $\lambda 6355$ is representative of the ejecta velocity at the photosphere, typically about $11,000 \text{ km s}^{-1}$ at B -band maximum (Benetti et al. 2005; Maeda et al. 2010; Wang et al. 2009, 2013). In some early spectra, there is a high velocity feature (HVF) of Si II $\lambda 6355$, detached from the PVF, which can be attributed to Si II absorptions formed in regions above the photosphere. Typical velocity of the HVF of Si II $\lambda 6355$ is about $18,000 \text{ km s}^{-1}$, while this HVF can reach above $30,000 \text{ km s}^{-1}$ for Ca II (Mazzali et al. 2005a,b; Tanaka et al. 2008; Silverman et al. 2015; Zhao et al. 2015, 2016; Li et al. 2020). The HVF of Si II $\lambda 6355$ usually only appears in early spectra, while the HVF of Ca II HK or Ca II NIR may also appear in some post-maximum spectra (Hatano et al. 1999;

* E-mail: zhaoxulin@139.com (TJUT)

Mazzali et al. 2005b; Childress et al. 2014; Maguire et al. 2014; Silverman et al. 2015). Our recent study revealed an anti-correlation between the properties of Si II $\lambda 6355$ HVF and those of the O I $\lambda 7773$ HVF (Zhao et al. 2016), which suggests that the HVFs may be associated with IME burnings in the outermost layers (see also, Kato et al. 2018; Mulligan & Wheeler 2017; Mulligan et al. 2019).

The strength of absorption features can be quantified with the pseudo-equivalent width (pEW; see, for example, Hachinger et al. 2006; Blondin et al. 2011) or the absorption depth normalized to the pseudo-continuum (see, for example, Nugent et al. 1995; Blondin et al. 2011). The excitation energy of the absorption feature is calculated by $E_{exc} = E_{upper} - E_{lower} = hc/\lambda$, where E_{lower} is the lower energy level, and E_{upper} is the upper energy level, λ is the rest-wavelength¹. The effect of E_{lower} can be seen from the strong absorptions of PVFs (photospheric-velocity feature) and HVFs of Si II $\lambda 6355$ and Ca II NIR (Zhao et al. 2015), while the effect of E_{exc} can be seen from comparison between lines Ca II HK and Ca II NIR, or between Si II $\lambda 4130$ and Si II $\lambda 5972$. The ionization degree also significantly affects the strength of absorption features, especially in 91T/99aa-like SNe (Mazzali et al. 1995; Fisher et al. 1999; Hachinger et al. 2008; Sasdelli et al. 2014; Taubenberger 2017).

While SNe Ia are known as standardizable candles, they actually have very diverse spectroscopic properties, including different velocity and strength of the observational features (including the HVFs), and presence/absence of some rare absorption features, such as variable sodium lines, H or He lines (e.g., Patat et al. 2007; Dilday et al. 2012; Jacobson-Galán et al., 2019). The photospheric temperature, which is associated with the amount of ^{56}Ni produced in the explosion (Nugent et al. 1995; Hoefflich et al. 1996; Mazzali et al. 2001; Kasen & Woosley 2007; Churazov et al. 2014), is considered to be the main cause for the spectroscopic diversity, but even two SNe Ia with similar brightnesses could exhibit very different spectral features (The opposite could also be the case; some SNe Ia with similar spectral features actually have significantly different peak luminosities; see, for example, Foley et al. 2020). Physically, the spectroscopic property of SNe Ia is determined by the initial chemical compositions of the WD progenitors (e.g., Hachinger et al. 2006; Nomoto et al. 2013), the explosion and burning modes (e.g., Whelan & Iben 1973; Nomoto 1982; Fink et al. 2010; Maeda et al. 2010; Bulla et al. 2016; Maguire et al. 2018), the birthplace environments (e.g., Wang et al. 2013; Mandel et al. 2017; Hill et al. 2018; Meng et al. 2019) and other factors. For example, the appearance of unburnt carbon feature C II $\lambda 6580$ may indicate a large amount of carbon in the WD progenitor (Parrent et al. 2011; Thomas et al. 2011; Folatelli et al. 2012; Silverman et al. 2012d; Hsiao et al. 2015), and tend to be related with the explosion mechanism/progenitor property (Li et al. 2020). The near-ultraviolet (NUV) features of SNe Ia were found to be strongly correlated with the progenitor metallicity

(Ellis et al. 2008; Mazzali et al. 2014; Brown & Crumpler 2020). The variable sodium or calcium feature reveals dense CSM around some SNe Ia (Hamuy et al. 2003; Patat et al. 2007; Sternberg et al. 2011; Maguire et al. 2013; Wang et al. 2019), which is in favor of the single-degenerate scenario (Whelan & Iben 1973; Nomoto 1982; Dilday et al. 2012). At the same time, there are also observational indications suggesting that the double-degenerate scenario may be responsible for some SNe Ia (e.g., Li et al. 2011; Schaefer & Pagnotta 2012; Kerzendorf et al. 2014); clearly more study is necessary in this respect.

Spectroscopic information could be used to improve the accuracy of distance determinations of SNe Ia, either through spectroscopic parameters that indicate the intrinsic diversities (Bailey et al. 2009; Wang et al. 2009; Foley & Kasen 2011; Maeda et al. 2011; Blondin et al. 2011; Silverman et al. 2012c; Burns et al. 2014; Mandel et al. 2014; Brown et al. 2018) or through others that reflect the explosion environments (Wang et al. 2013; Anderson et al. 2015; Hill et al. 2018). For example, Wang et al. (2009) found that the SN Ia subclass with high Si II $\lambda 6355$ velocities ($v \geq 11,800 \text{ km s}^{-1}$, HV) near B -band maximum² and the subclass with normal Si II $\lambda 6355$ velocities ($8,000 < v < 11,800 \text{ km s}^{-1}$, NV) near B -band maximum have different observed colors. Using different extinction ratios for the two subclasses reduced the luminosity dispersion from 0.178 mag to 0.125 mag. Also, there are some studies showing intrinsic correlation between the velocity and the light curve time scale (Zhang et al. 2010; Ganeshalingam et al. 2011; Kawabata et al. 2020). Some characteristic features, i.e., C II $\lambda 6580$ absorption, may help select a subsample of “well-behaved” SNe Ia for more precise distance measurements (Parrent et al. 2011; Thomas et al. 2011; Folatelli et al. 2012; Silverman et al. 2012d).

Previous studies of the spectral features mostly focus on near-maximum light epochs (e.g., Branch et al. 2006; Hachinger et al. 2006; Wang et al. 2009; Blondin et al. 2011; Silverman et al. 2012b,c). Due to the lack of early-time spectra ($t \lesssim -7 \text{ d}$), study on early-time spectral behaviors of SN Ia is still limited. Some information, such as features from unburnt materials, are often seen in the early phase. Different models usually predict similar maximum spectra; the early spectral information can be a key to further constrain explosion models (e.g., Maeda et al. 2018). A comparison between features of early time and near maximum light tells much about the influences of temperature, luminosity, and change in element abundances, which forms a fundamental problem for interpreting the spectral diversity of SN Ia (e.g., Blondin et al. 2012; Folatelli et al. 2013; Maguire et al. 2014; Stahl et al. 2020). A comparison between different features also provides important clues about the physics behind the spectral diversity of SN Ia. In this work, we collect a large sample of early spectra of SNe Ia as well as spectra near maximum light, and carefully examine the evolutions of four important spectral features Si II $\lambda\lambda 4130, 5972, 6355$ and S II W-trough. We also examine the differences and correlations between these features, and their

¹ A table of the energy levels of important lines in spectra of SNe Ia near maximum light can be found on website: <http://supernova.lbl.gov/~dnkasen/tutorial/>

² Throughout this paper the maximum is referred to the B -band maximum.

dependences on the SN brightness. We address many details of the evolutions of these spectral features, and the results may be useful for future studies of SN Ia spectroscopy and SN Ia cosmology.

This paper is organized as follows. In Section 2 we present the spectroscopic sample used in this study, and describe our measurement procedure. Section 3 presents the temporal evolutions of the velocities and pEWs for different subclasses, and explore the correlation between velocity and pEW. In Section 4 we focus on the link between spectral properties and the luminosity decline rate $\Delta m_{15}(B)$ ³. In Section 4 we also examine the temporal evolutions of the velocity-differences and depth-ratios between different features, and present the evolutions of correlations of several possible spectral luminosity indicators with $\Delta m_{15}(B)$. In Section 3 and 4, the physical implications of our observational results are also discussed. We close the paper in Section 5 with our concluding remarks.

2 DATA AND MEASUREMENTS

Data source: Most spectra used in this work were compiled from the CfA supernova program (Matheson et al. 2008; Blondin et al. 2012), the Berkeley supernova program (Silverman et al. 2012a,b; Stahl et al. 2020) and the Carnegie Supernova Project (CSP, Folatelli et al. 2013). These SNe Ia are mostly included in our previous study (Zhao et al. 2015), where more information can be found. Photometric parameters are taken from the literature. After $t \approx +6$ d⁴, serious blends and spectral distortions make it difficult to perform an accurate measurement for most features of Si II and S II. Therefore our sample includes only spectra taken before +6 d. All spectra cover the wavelengths of the absorption features Si II $\lambda\lambda 5972$, 6355 and S II W-trough (5,300 – 6,000 Å).

Sample selection: The original database contains more than 5,000 spectra of SNe Ia, but only about 2,000 spectra (from about 400 SNe Ia) were obtained before +6 d. We further selected about 120 SNe Ia which have at least 5 spectra at different phases between –15 and +5 d. The purpose of selecting relatively extensively observed SNe is to reduce the influence of the SN diversity on the mean evolutions. If using different objects at different phases, the evolutionary trends could be covered by the SN diversity, especially for those with slow evolutions. To take an extreme example, suppose we would use a sample including only two spectra from SN 1998aq at –9.2 d ($V_{Si6355} = 10,944$ km s^{–1}) and SN 2003cg at –6.2 d ($V_{Si6355} = 11,530$ km s^{–1}), a false-increasing trend of V_{Si6355} appears. Also, for most objects, we used spectra from one source to avoid systematic error. This additional selection criteria further reduced the sample size to 105 SNe Ia. Furthermore, there were other problems such as poor spectra quality (i.e., low signal-to-noise ratio), too complex continuum, strong line contamination, insufficient wavelength coverage, or unsuitable phase distribution

(for example, for SN 2000fa we have 5 spectra at –11, –9, +1, +2 and +4 days, but these data hardly reveal details of the evolutionary trend). By considering the above factors, we obtained our final sample with 79 SNe Ia.

The rest-wavelengths of the two components of S II W-trough: Multiple lines contribute to the absorption feature of S II W-trough, merging together as a doublet absorption. The rest-wavelength of the bluer component is usually taken to be 5454 Å. The rest-wavelength of the redder component, however, has been disputed, and most people use 5640 Å (e.g., Hachinger et al. 2006; Blondin et al. 2011). In this work, we also use 5454 Å as the rest-wavelength of the bluer component, but 5620 Å for the redder component. The adoption of 5620 Å rest-wavelength was calculated by $(1.43219 \times 5606.15 \text{ \AA} + 1.40281 \times 5640.35 \text{ \AA}) / (1.43219 + 1.40281) \approx 5620 \text{ \AA}$, where 5606.15 and 5640.35 Å are the wavelengths of the two lines that blend into the redder component of S II W-trough, and 1.43219 and 1.40281 are the corresponding oscillator strengths, respectively. Using 5620 Å rest wavelength for the redder component leads to a mean velocity difference of about 400 km s^{–1} between these two components, while using 5640 Å rest wavelength leads to a mean velocity difference of about 1,400 km s^{–1}. Since two lines with very similar energy levels are expected to have very similar velocities, it is more physically plausible to use 5620 Å as the rest wavelength of the redder component of S II W-trough (E_{lower} : 13.73 eV vs. 13.70 eV, E_{exc} : 2.21 eV vs. 2.27 eV).

Smoothing: Before fitting, we smoothed each observed spectrum with a locally weighted linear regression (nearer neighbors were more heavily weighted; see, for example, Cleveland 1979). For fittings of S II W-trough and Si II $\lambda\lambda 5972$, 6355, the smoothing window was 125 – 150 Å. This span effectively reduces the influence of noise, and also well preserves the profiles of the features. For Si II $\lambda 4130$, the span is much smaller (≈ 35 Å). This well preserves the details of Si II $\lambda 4130$ which could be very weak at early times.

Pseudo-continuum: As demonstrated in Figure 1, the pseudo-continua are defined by connecting the featureless points in the spectrum. Note that the two ends of a feature are not necessarily featureless, because there could be serious blending between two neighboring features. For example, the red end of Si II $\lambda 5972$ of SN 2004as in Figure 1 is much lower than the straight line that well fit the featureless points near 5400, 5850 and 6600 Å. The red end of S II $\lambda 5620$ of SN 2004ef shows a similar behavior, as shown in Figure 1. For some spectra at early times, more sophisticated method for determining the pseudo-continuum is required if a “perfect” fitting is desired. This is however beyond the scope of this paper, and this does not affect the conclusions of this work. For most spectra, the pseudo-continuum is well-fitted by the classical method, i.e., connecting featureless points. In Figure 1, typical examples of the pseudo-continuum are shown. In some cases the pseudo-continuum (between 5,400 and 6,500 Å) appears to be linear, while in other cases the pseudo-continuum appears to be “Λ”-shape (e.g., 2004eo at –10.4 d) or “V”-shape (e.g., 2004ef at –6.7 d).

Spectral fitting: The measurement procedure is overall similar to that applied in our previous works (Zhao et al. 2015, 2016). The Si II $\lambda 4130$ feature was fitted with a single-gaussian model. S II W-trough, Si II $\lambda\lambda 5972$ and 6355, HVF of Si II $\lambda 6355$, C II $\lambda 6580$ and an unknown feature near

³ Defined as the change in B -band magnitude from peak to 15 days after that in the rest-frame of the SN (Phillips 1993).

⁴ Throughout this paper the spectral phases correspond to the rest-frame days relative to the B -band maximum. All time intervals in this paper are also in rest-frame days.

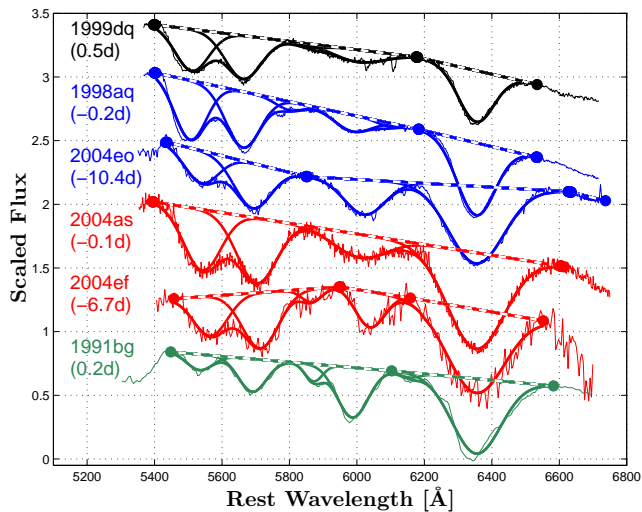


Figure 1. Gaussian fits to the absorption features of Si II $\lambda\lambda 6355$, 5972 and S II W-trough in the optical spectra of some representative SNe Ia near maximum light. Color coded by subclasses of Wang et al. (2009) are spectra of NV (blue) SNe 1998aq and 2004eo, HV (red) SNe 2004as and 2004ef, 91T/99aa-like (black) SN 1999dq and 91bg-like (sea-green) SN 1991bg. The fluxes have been normalized, redshift-corrected and additive offsets applied for clarity, and labeled by phases with respect to B -band maximum light. The large dots mark the points that were considered to be featureless. The pseudo-continua were then constructed by connecting them with straight lines (marked with dash-lines). Si II $\lambda 4130$ is truncated off the plot to focus on the region covered by more complex fitting.

5600 Å were fitted consistently and simultaneously with a 7-component gaussian function. In most cases, these features were well-separated by applying velocity constraints. For example, S II $\lambda 5454$ with velocity $7,000 \leq V_{S5454} \leq 12,000$ km s^{-1} is located at $5240 \leq \lambda_{S5454} \leq 5328$ Å, while its neighboring feature S II $\lambda 5620$ with similar velocity is located at $5400 \leq \lambda_{S5620} \leq 5490$ Å. This means the two components of the S II W-trough will never be mistaken. All fittings were visually inspected to ensure that a good fit was obtained. The velocity and line strength measurements are listed in Table 1.

Measurement uncertainties: The smoothed-and-interpolated spectra (using “linear-interpolation” method in MATLAB, with 0.5 Å interval) are generally well fitted by the multiple-gaussian function, with the coefficient of determination (R-squared) ranging from 0.925 to 0.999. However, for each component the uncertainty could be much higher due to the blendings. The uncertainties (for each component) are given in Table 1. They are the total uncertainties with contributions from the gaussian fitting, the flux error, and the wavelength uncertainty (depending on the wavelength interval).

3 TIME EVOLUTION OF THE SI II AND S II FEATURES

3.1 Temporal evolution of line velocity

The velocity of a given feature is derived from the blueshift of its deepest absorption (i.e., the minimum of the fea-

ture after the pseudo-continuum is removed) relative to the rest-wavelength. Each feature in the spectrum has its own velocity, depending on where the absorption is located in the ejecta (e.g., Patat et al. 1996). The velocity evolution of Si II $\lambda 6355$ has been studied intensively (e.g., Benetti et al. 2005; Wang et al. 2009; Foley et al. 2011; Blondin et al. 2012), while the velocity evolution for other lines may need further investigation. Velocity evolutions of lines Si II $\lambda\lambda 4130$, 5972 and S II W-trough have been studied by, e.g., Silverman et al. (2012b), Folatelli et al. (2013), and Stahl et al. (2020). Our sample is most similar to that of Blondin et al. (2012), who did not give these velocity evolution measurements. Below we present the velocity evolutions for these lines as well as Si II $\lambda 6355$.

Figure 2 shows the velocity evolutions for different subclasses in the Wang et al. (2009) classification scheme. For each point, we took the mean of the measurements within ± 0.5 d, i.e. $t \pm 0.5$ d. In general, the velocities decrease with time as expected (due to the recession of the photosphere following the expansion and the decrease in density). The only exception is the velocity of Si II $\lambda 5972$ (V_{S5972}), which somehow surprisingly increases with time after $t \approx -2$ d, and even surpasses the velocity of Si II $\lambda 6355$ (V_{S6355}) after $t \approx +2$ d (see discussion in §4.6). No systematic bias was found in the analysis method that could cause the abnormal behavior of V_{S5972} .

During the phase from $t \approx -14$ to $+5$ d, the NV objects have an average velocity gradient of about 200 km $s^{-1}d^{-1}$, while the HV objects have corresponding value of about 300 km $s^{-1}d^{-1}$, and the 91T/99aa-like objects (Filippenko et al. 1992b; Phillips et al. 1992; Li et al. 2001; Garnavich et al. 2004; Sasdelli et al. 2014; Taubenberger 2017) have an average velocity gradient of about 100 km $s^{-1}d^{-1}$. During the phase from $t \approx -7$ to $+3$ d, the representative 91bg-like (Filippenko et al. 1992a; Mazzali et al. 1997; Howell et al. 2001; Hachinger et al. 2009; Taubenberger 2017) object, SN 1998de is found to have a velocity gradient of about 400 km $s^{-1}d^{-1}$. It is clear that faster decliners tend to have more rapidly declining velocities, possibly due to their faster decreases in temperature.

Velocities obtained here are generally consistent with previous studies, including the rising trend of V_{S5972} after B -band maximum (e.g., Silverman et al. 2012b). We use a sample that is most similar to Blondin et al. (2012). The V_{S6355} measured around the B -band maximum is about 11,000 km s^{-1} for normal SNe Ia in Blondin et al. (2012), compared to about 10,600 km s^{-1} obtained in our work. Minor difference could be due to two reasons: Firstly, the determination of the position of the absorption minima. Whether it is directly determined from the smoothed flux or determined by a gaussian fitting can lead to different results in the velocity measurement. Secondly, the blending of some features (e.g., Si II $\lambda 6355$ at early times) with other lines or the HVF may also seriously affect the velocity measurement (e.g., Zhao et al. 2015).

3.2 Temporal evolution of line strength

The absorption strength can be quantified by the pseudo-equivalent width (pEW, see, e.g., Blondin et al. 2011; Zhao et al. 2015, for details), or the absorption depth (H)

Table 1. Measured velocities and line strengths. This is a sample of the full table, which is available online (see ‘‘Supporting Information’’).

SN	Phase ^a (d)	Subtype ^b	$\Delta m_{15}(B)^c$ (mag)	V_{Si}^{4130d} (km s ⁻¹)	W_{Si}^{4130e} (Å)	V_{Si}^{5972f} (km s ⁻¹)	W_{Si}^{5972g} (Å)	V_{Si}^{6355h} (km s ⁻¹)	W_{Si}^{6355i} (Å)	V_S^{5454j} (km s ⁻¹)	W_S^{5454k} (Å)	V_S^{5620l} (km s ⁻¹)	W_S^{5620m} (Å)	Src ⁿ	Ref. ^o
1994D	-11.5	NV	1.37	11447(573)	10(1)	12177(609)	57(4)	13677(684)	139(3)	10285(515)	28(2)	11022(552)	44(2)	CfA	1
1994D	-9.5	NV	1.37	10321(517)	14(2)	11575(579)	29(1)	12395(620)	102(3)	10250(513)	31(3)	10924(547)	42(2)	CfA	1
1994D	-8.5	NV	1.37	10597(530)	19(2)	11370(569)	23(2)	12169(609)	105(3)	10398(520)	27(2)	11083(555)	37(2)	CfA	1
1994D	-4.5	NV	1.37	10351(518)	19(2)	10847(543)	18(2)	11584(580)	95(7)	9610(481)	31(3)	10153(508)	35(3)	CfA	1
1994D	-2.5	NV	1.37	10067(504)	23(1)	10603(531)	19(2)	11054(553)	97(7)	9362(469)	38(3)	9852(493)	39(3)	CfA	1
1994D	1.5	NV	1.37	9962(499)	23(1)	10782(540)	24(2)	10888(545)	104(8)	8770(439)	40(3)	9322(467)	45(2)	CfA	1
1994D	2.5	NV	1.37	–	–	11197(560)	31(3)	10813(541)	106(8)	8544(428)	42(4)	9252(463)	54(2)	CfA	1
1994D	3.5	NV	1.37	9146(458)	20(1)	11246(563)	34(3)	10746(538)	109(9)	8353(418)	42(4)	8824(442)	56(2)	CfA	1
1994D	4.5	NV	1.37	–	–	11293(565)	32(2)	10793(540)	106(8)	8361(419)	38(3)	8788(440)	51(2)	CfA	1

Notes. Uncertainties are listed in parentheses.

^a Phases of spectra are in rest-frame days relative to the time of B -band maximum light.

^b Wang-scheme classification (Wang et al. 2009). The velocity boundary between HV-SNe and NV-SNe is around 11,800 km s⁻¹.

^c B -band light-curve decline rate $\Delta m_{15}(B)$.

^d Velocity of Si II λ 4130, for the photospheric (PHO) component;

^e Pseudo-equivalent width of Si II λ 4130, for the PHO component;

^f Velocity of Si II λ 5972, for the PHO component;

^g Pseudo-equivalent width of Si II λ 5972, for the PHO component;

^h Velocity of Si II λ 6355, for the PHO component;

ⁱ Pseudo-equivalent width of Si II λ 6355, for the PHO component;

^j Velocity of S II λ 5454, for the PHO component;

^k Pseudo-equivalent width of S II λ 5454, for the PHO component;

^l Velocity of S II λ 5620, for the PHO component;

^m Pseudo-equivalent width of S II λ 5620, for the PHO component;

ⁿ Data source References: CfA- CfA supernova program (Matheson et al. 2008; Blondin et al. 2012); Lick- Berkeley Supernova Program (Silverman et al. 2012a,b; Stahl et al. 2020); CSP- Carnegie Supernova Project (CSP Folatelli et al. 2013); THU- Tsinghua Supernova Program (Zhang et al. 2015a); Alt07 = (Altavilla et al. 2007); Chi13 = (Childress et al. 2013); Per13 = (Pereira et al. 2013); Zha15 = (Zhang et al. 2015b); Zhe13 = (Zheng et al. 2013). Most of the spectra are available on the online ‘‘open supernova catalog’’ (Guillochon et al. 2017);

^o Photometric References: 1 = (Blondin et al. 2012); 2 = (Brown et al. 2019); 3 = (Childress et al. 2013); 4 = (Childress et al. 2014); 5 = (Folatelli et al. 2012); 6 = (Folatelli et al. 2013); 7 = (Ganeshalingam et al. 2010); 8 = (Jha et al. 2006); 9 = (Pignata et al. 2004); 10 = (Silverman et al. 2015); 11 = (Stritzinger et al. 2011); 12 = (Wang et al. 2009); 13 = (Zhang et al. 2015b); 14 = (Zheng et al. 2017);

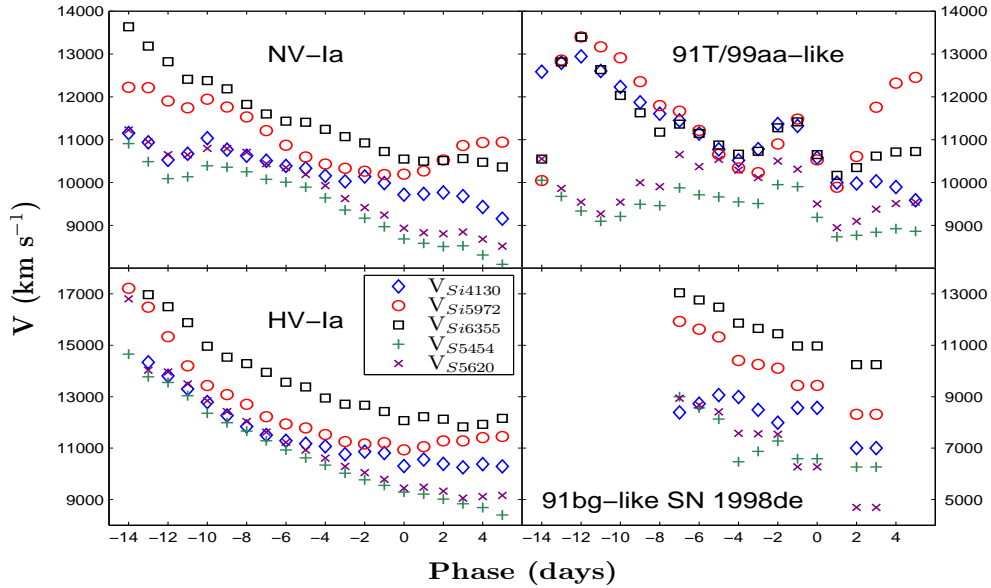


Figure 2. Evolutions of the velocities (V) with time for the four subclasses defined by Wang et al. (2009). The velocities are averaged over 1 d intervals. Color coded are the four lines we study: Si II λ 4130 (blue diamond); Si II λ 5972 (red circle); Si II λ 6355 (black square); the two components of S II W -trough (green/brown). Due to lack of extensively observed 91bg-like objects, we can only use SN 1998de as a representative. Note that the y-axis ranges have been increased in the bottom panels to encompass the larger variations in the velocities of HV and 91bg-like SNe.

which is defined as the deepest absorption of the feature normalized to the pseudo-continuum. The temporal evolutions of the pEWs of Si II λ 4130, 5972, 6355 and S II W -trough have been studied by, e.g., Silverman et al. (2012b), Folatelli et al. (2013), and Stahl et al. (2020), but not given by Blondin et al. (2012). As mentioned previously, our sample is very similar to that of Blondin et al. (2012), and below we present the pEW evolutions for our sample.

Figure 3 shows the pEW evolutions for different subclasses in the classification scheme proposed by Wang et al. (2009). Each point was averaged over 1 d intervals, i.e. $t \pm 0.5$ d. *NV objects*: In general, the pEWs of NV objects increase with time before the B -band maximum. An exception for this tendency is pEW of Si II λ 5972, which decreases until $t \approx -1$ d. The other longer-wavelength feature, Si II λ 6355, also weakens with time before $t \approx -7$ d, then slowly increases until $t \approx -4$ d, after which it remains vir-

tually unchanged. It appears from Figure 3 that the pEW of S II W-trough of NV objects reaches a maximum value near $t \approx +2$ d, though the trend is less noticeable than in 1991T/99aa-like SNe Ia. For Si II $\lambda 4130$, though the average pEW shows a slight trend of increasing after $+2$ d, there are actually more than half of NV objects exhibiting a decrease or plateau of pEW after $t \approx +2$ d. Specifically, after $+2$ d, SNe 1994D, 2002er, 2003cg and 2005cf show a decreasing pEW, SNe 1998aq, 2004at, 2005el, 2006le and 2011fe show constant pEW, while SNe 2002de, 2003du, 2006S, 2007af, 2008ar, 2008bf and 2009ab show a slowly increasing pEW (see Table 1).

The delay in reaching the maximum line-strength relative to the maximum light could be due to our using B -band maximum light as the 0 d, as V -band maximum is usually 1 - 2 d later than the B -band maximum. We notice that Si II $\lambda 5972$ behaves differently than other features, with a minimal pEW near $t \approx -1$ d (see discussion in §4.6). The fact that the features generally reach an extremum (i.e., maximum or minimum) pEW near maximum light suggests that the line strengths are significantly influenced by the luminosity. However some features (i.e., Si II $\lambda 6355$) seem not to follow the trend. This can be explained as other factors such as saturation, temperature, element abundance, which can also affect the absorption strengths.

Other subtypes: HV objects are characterized by large and nearly constant line strengths of Si II $\lambda 6355$ and S II W-trough, which may imply a high degree of saturation. The evolutionary trends of the velocities and the pEWs of HV SNe are overall similar to those of NV SNe, supporting the classification of both “HV-Ia” and “NV-Ia” objects as “normal” SNe Ia. The 91T/99aa-like objects are characterized by weak Si II $\lambda 6355$ and nearly constant strength of Si II $\lambda 4130$.

The evolutionary trends we showed above are generally consistent with the results given by some recent studies (Silverman et al. 2012b; Folatelli et al. 2013; Stahl et al. 2020), except for pEW_{Si5972} . Our results are similar to that of Folatelli et al. (2013), with a decreasing trend of pEW_{Si5972} before B -band maximum. In Stahl et al. (2020), four-day mean value of pEW_{Si5972} slightly decreases from 20 \AA to 17 \AA at $-17 < t < -9$ d, but it then increases progressively from 17 to 25 \AA at $-9 < t < +5$ d. Stahl et al. (2020) also gives the four-day mean value of pEW_{Si5972} using the data from Silverman et al. (2012b), which increases from 18 to 26 \AA at $-12 < t < -5$ d, it then remains nearly unchanged between -5 and $+5$ d ($\approx 26 \text{ \AA}$). The discrepancy may be due to the different sample or different measurement method (see discussion in §2). Nevertheless, our measurement of pEW_{Si5972} is still roughly consistent with the previous studies. For example, at B -band maximum, Silverman et al. (2012b) give a mean value of $pEW_{Si5972} \approx 25 \text{ \AA}$ for normal SNe, while we give a corresponding value of $\approx 23 \text{ \AA}$. At -5 d, Silverman et al. (2012b) give a mean value of $\approx 26 \text{ \AA}$ for normal SNe, while we give $pEW_{Si5972} \approx 25 \text{ \AA}$.

3.3 Correlation between velocity and line strength

The correlation between V_{Si6355} and pEW_{Si6355} has been previously studied by, e.g., Wang et al. (2009), Blondin et al. (2012) and Maguire et al. (2014). In

Wang et al. (2009), a clear trend of larger pEW corresponding to higher velocity at maximum light was observed in both NV and HV subclasses. In Blondin et al. (2012), HV SNe show positive velocity-pEW correlation, while NV SNe show no clear velocity-pEW correlation. In Maguire et al. (2014), HV SNe show no clear velocity-pEW correlation, while NV SNe show a slight trend with larger pEW corresponding to larger velocity. The discrepancy between these results may be due to sample selection. Also note that the correlation could be seriously affected by the evolutionary effect, depending on how velocity and pEW evolve in the phase range. In this section, we do not reinvestigate the velocity-pEW correlation at maximum light, but instead focus our analysis on the evolution of this correlation.

Figure 4 shows the correlation between velocity and pEW for Si II $\lambda 6355$ and S II W-trough. The data are restricted to be within ± 2 d from the selected epochs to reduce the evolutionary effect: left panels are for the sample at -6 ± 2 d, right panels of the same figure are for the sample at 3 ± 2 d. The overall trend is positive, but mainly due to the fact that HV SNe generally have both higher velocities and pEWs than the NV counterparts. Within each subclass, the exact correlation seems to depend on the phase.

For Si II $\lambda 6355$ in the spectra of HV or 91T/99aa-like SNe, the velocity and pEW appear to be positively correlated near $t \approx -6$ d, but this correlation becomes weak near $+3$ d. The reason of the positive velocity-pEW correlation near $t \approx -6$ d is unclear. Physically, the velocity and pEW may not affect each other directly, but they might be indirectly connected through temperature, luminosity or element abundance. For the NV SNe, the velocity-pEW correlation of Si II $\lambda 6355$ is weak if there is any near -6 d, and seems to show a negative correlation near $t \approx +3$ d. A negative correlation can be explained as a result of lower optical depth in outer layers, in addition to the relatively high degree of homogeneity within NV-Ia subclass, which reduces the effect of element abundance and luminosity. Negative velocity-pEW correlation is also seen in both photospheric and HVF components of O I $\lambda 7773$ (Zhao et al. 2016). The change in $V_{Si6355} - pEW_{Si6355}$ may be related to the changes in $\Delta m_{15}(B)$ -dependence of V_{Si6355} and pEW_{Si6355} . At $t \approx +3$ d, possibly due to decrease in temperature, V_{Si6355} becomes anti-correlated with $\Delta m_{15}(B)$, while pEW_{Si6355} is positively correlated with $\Delta m_{15}(B)$ (see §4.1 and 4.2 for more details).

For S II W-trough near $t \approx -6$ d, the velocity-pEW correlation appears to be insignificant within the HV or 91T/99aa-like objects, and it may be negative for the NV objects. This negative correlation for NV objects somehow disappears near $t \approx +3$ d, as shown in the bottom-right panel of Figure 4. This may be due to a negative correlation between V_{SW} and $\Delta m_{15}(B)$, which is weak at $t \approx -6$ d, but strong at $t \approx +3$ d (discussed later in §4.1 and 4.2).

3.4 Comparison between 91T/99aa-like and 91bg-like SNe

The effects of the temperature on the absorption features have been introduced in §1. Here, we make comparison between the “hot” 91T/99aa-like objects and the “cool” 91bg-like objects to see the details. (a) As shown in Figure 2, the velocities of 91T/99aa-like objects stay almost unchanged after $t \approx -8$ d relative to B -band maximum. In contrast,

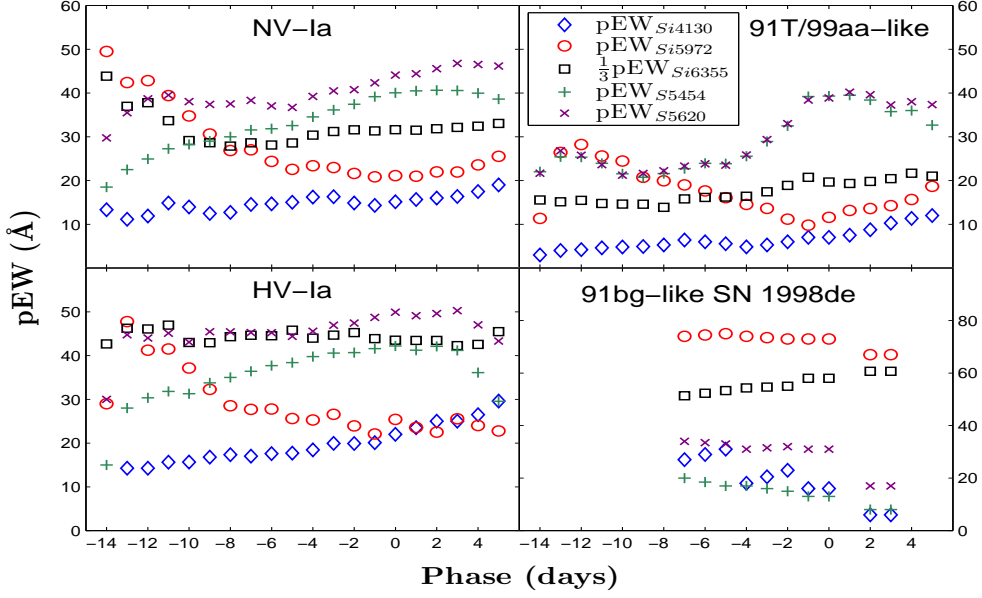


Figure 3. Evolutions of the pseudo-equivalent widths (pEWs) with time for the four spectroscopic subclasses defined by Wang et al. (2009). The pEWs are averaged over 1 d intervals. Due to lack of extensively observed 91bg-like object, we can only use SN 1998de as representative. Colors and shapes of data points are the same as in Figure 2.

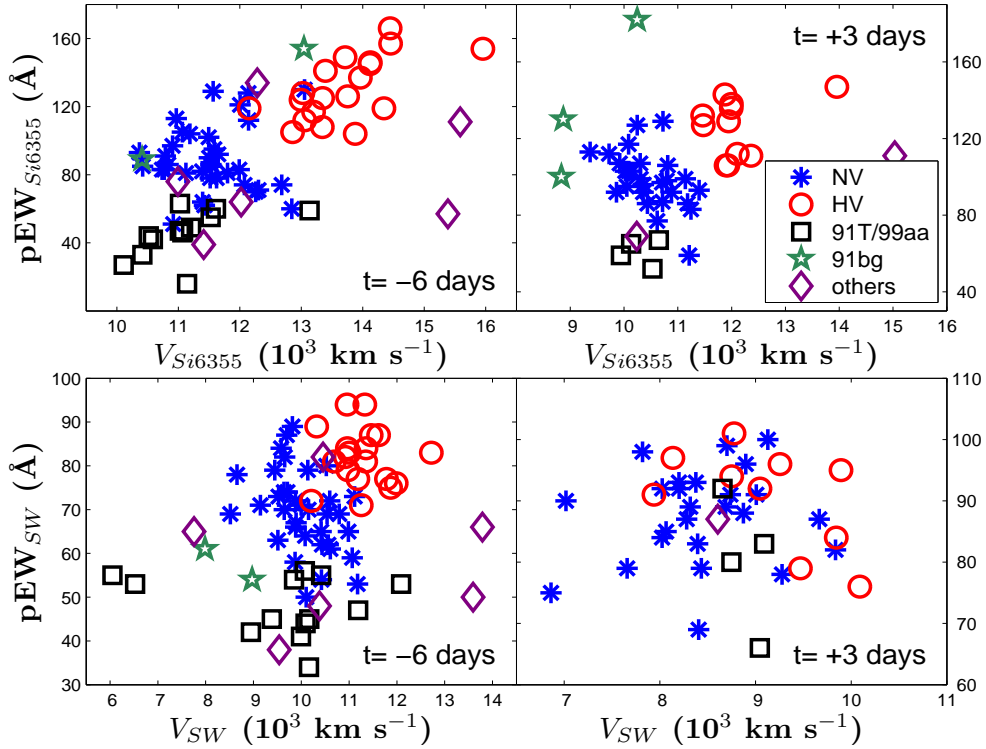


Figure 4. Top-left panel: pEW of the Si II $\lambda 6355$ feature as a function of the velocity of Si II $\lambda 6355$ feature for SN Ia spectra within 2 d of -6 d since maximum light. If more than one measurement was available, the one closest to the central phases was used. Bottom-left panel: Similar to the top-left panel, but for the S II W-trough feature. Right panels: Similar to the left panels, but for spectra near $+3$ d. The sample has been split into subclasses as defined by Wang et al. (2009). Blue asterisks are normal-velocity (NV) objects, red circles are high-velocity (HV) objects, black squares are 91T/99aa-like objects, green pentagrams are 91bg-like objects. Other objects, including peculiar or uncertain subtype objects are marked with brown diamond.

the velocities of 91bg-like objects decrease rapidly with time; (b) As shown in Figure 3, the pEWs of 91T/99aa-like objects keep increasing with time. On the other hand, the pEWs of 91bg-like objects keep decreasing with time, except for the lowly excited feature Si II $\lambda 6355$. (c) As shown in Figure 4 (which shows relations between the velocities and pEW or Si II $\lambda 6355$ and S II W-trough at different epochs), 91T/99aa-like objects have much weaker Si II $\lambda 6355$ but much stronger S II W-trough than 91bg-like objects. These may serve as an example of temperature effect, which is important for understanding the spectral diversity, as will be further discussed in the next section.

4 THE DECLINE-RATE DEPENDENCES OF THE SI II AND S II FEATURES

4.1 The decline-rate dependence of the velocity

While some studies (Hatano et al. 2000; Benetti et al. 2005; Foley et al. 2011) suggested no clear correlation between the velocity of Si II $\lambda 6355$ at B -band maximum and $\Delta m_{15}(B)$, others suggest that the velocity at B -band maximum is anti-correlated with $\Delta m_{15}(B)$ (Hachinger et al. 2006). In this section, we show how the velocity- $\Delta m_{15}(B)$ correlation evolves with time.

Figure 5 shows the Pearson correlation coefficients (ρ , as defined in Eq. 1) between the velocities and the $\Delta m_{15}(B)$. The negative Pearson coefficients suggest that the velocities are generally anti-correlated with the $\Delta m_{15}(B)$. The Pearson coefficients are mostly very small, suggesting that the correlations are modest, insignificant or even nonexistent at most phases. The Pearson correlation coefficient is defined as follows:

$$\rho_{x,y} = \frac{\text{cov}(x,y)}{\sigma_x \sigma_y} = \frac{\sum_{i=1}^n (x_i - \bar{x})(y_i - \bar{y})}{\sqrt{\sum_{i=1}^n (x_i - \bar{x})^2 \sum_{i=1}^n (y_i - \bar{y})^2}}, \quad (1)$$

where σ_x , σ_y are the standard deviations of x and y , respectively, and $\text{cov}(x,y)$ is the covariance between x and y .

Figure 5 also shows how the correlations evolve with time. The correlations are very weak at early times, they then grow stronger with time until +4 d, implying a stronger dependence of the velocity on $\Delta m_{15}(B)$ at cooler temperature. For some reason the correlations between the velocities and $\Delta m_{15}(B)$ weaken with time after +4 d. The correlation is strongest for S II W-trough, and weakest for Si II $\lambda 6355$, implying a stronger dependence on the SN brightness for lines from highly-excited levels. A relatively strong correlation seems to exist between V_{SW} at $t \approx +3$ d and $\Delta m_{15}(B)$, as shown in the bottom-right panel of Figure 6.

When the sample is restricted to only a subclass, the correlation of the velocity with $\Delta m_{15}(B)$ appears somewhat weaker. In fact, as shown in Figure 6, the correlation is largely driven by 91bg-like objects which have both lower velocities and luminosities than other subclasses. This may explain the relatively strong velocity- $\Delta m_{15}(B)$ correlation in Hachinger et al. (2006), as their sample contains a higher fraction of SN 91bg-like events.

At -6 d, line velocities of 91T/99aa-like SNe seem to have stronger correlations with $\Delta m_{15}(B)$ than that of other subclasses, as shown in Figure 6. This may be due

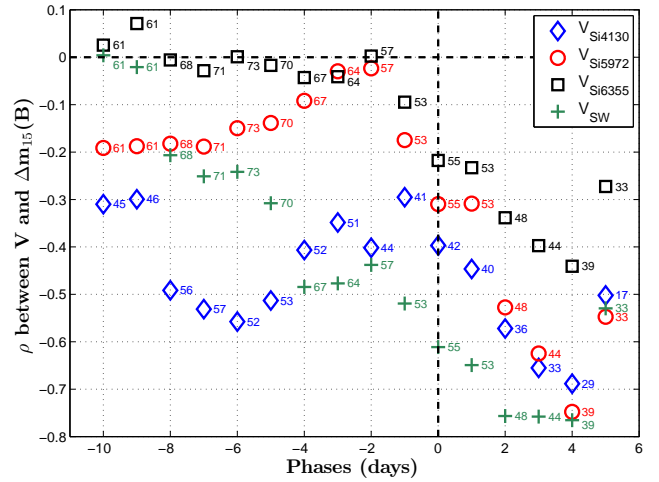


Figure 5. Time-evolutions of the Pearson correlation coefficients between the velocities and $\Delta m_{15}(B)$. Measurements within 2 d were used, and if more than one measurement was available, the one closest to the central phases was used. The whole sample, including NV, HV, 91T/99aa-like and 91bg-like SNe are all included.

to a more significant ionization effect in 91T/99aa-like object, as their photospheric temperatures are relatively high (Benetti et al. 2005). A higher degree of ionization can cause the singly ionized absorptions to move outward to the cooler, faster-moving layers, and thereby an anti-correlation between the velocity and $\Delta m_{15}(B)$. It is also noted that V_{SW} appears to have a stronger correlation with $\Delta m_{15}(B)$ than V_{Si6355} . For example, at -6 d, when $\Delta m_{15}(B)$ increases from 0.8 to 1.0 mag, V_{SW} (of 91T/99aa-like SNe) decreases from 12,000 to 6,000 km s⁻¹, while V_{Si6355} (of 91T/99aa-like SNe) only decreases from 13,000 to 10,000 km s⁻¹, as shown in the left panels of Figure 6 (see also the discussion in §4.3). A possible reason is the relatively high energy levels of S II W-trough, which makes the line more sensitive to the photospheric temperature.

4.2 The decline-rate dependence of the line strength

Hachinger et al. (2006) and Blondin et al. (2012) have studied the correlation between pEW and $\Delta m_{15}(B)$ for various lines at maximum light, with the aim to find better spectroscopic luminosity indicator. In this section, we further explore the temporal evolutions of the correlations between the line strengths and the $\Delta m_{15}(B)$, and compare them among different subclasses of SNe Ia. Unlike most studies, here we use the absorption depth (H) to represent the line strength, as it shows a slightly stronger correlation with $\Delta m_{15}(B)$ (see §4.5 for more details).

Figure 7 shows positive correlations between the depths of Si II and S II absorption features and $\Delta m_{15}(B)$. The sample is restricted to NV-SNe Ia whose high degree of homogeneity (meaning relatively similar velocities and line strengths of IME features, as well as relatively similar luminosities) leads to a tighter relation with $\Delta m_{15}(B)$. One possible explanation for the positive correlations is that the dimmer objects tend to suffer less burning and have hence more IME left in the ejecta. Another possible reason is that

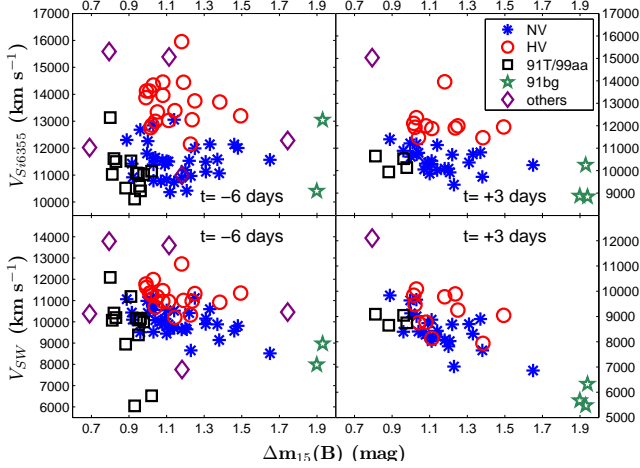


Figure 6. Velocities of Si II $\lambda 6355$ and S II W-trough at -6 and $+3$ d as a function of $\Delta m_{15}(B)$. Measurements within 2 d were used, and if more than one measurement was available, the one closest to the central phase was used. Colors and shapes of data points are the same as in Figure 4.

in dimmer objects the photospheric temperature is relatively low, in favor of low-ionization lines such as Si II $\lambda 6355$.

It is somewhat surprising that dimmer objects display stronger absorptions in Si II $\lambda\lambda 4130, 5972$ and S II W-trough than brighter objects, since these lines originate from rather highly excited levels. These positive correlations between the line strengths and $\Delta m_{15}(B)$, together with the pEW-evolutions (see §3.2), seem to suggest a less importance of temperature effect on those prominent features than the luminosity. Nonetheless, the correlation is weak for Si II $\lambda 6355$ which has the lowest excitation energy, and also weak for S II W-trough which has the highest excitation energy, suggesting that only the lines with proper (excitation & ionization) energies may have a strong correlation with the peak brightness.

In the left panels of Figure 8, we compare the decline-rate dependence of pEW_{Si6355} at $t \approx -6$ d to that of pEW_{SW} . Although these two lines are produced with very different excitation and ionization energies, it appears that their pEWs have similar correlations with $\Delta m_{15}(B)$. For NV SNe, the pEWs appear to be positively correlated with $\Delta m_{15}(B)$, which has been discussed in the previous paragraph. For HV SNe which have relatively large pEWs, the pEW- $\Delta m_{15}(B)$ correlation is insignificant.

In 91T/99aa-like SNe, as shown in Figure 8, the pEWs of both Si II and S II lines appear anti-correlated with the decline rate, i.e., brighter 91T/99aa-like objects tend to have stronger absorptions of Si II $\lambda 6355$ and S II W-trough. This is rather puzzling because brighter 91T/99aa-like objects are expected to have more complete burning of IME to ^{56}Ni . It may not be a result of either temperature effect or luminosity effect, because a dimmer/colder condition prefers the formation of Si II $\lambda 6355$. A possible explanation is that oxygen burning in 91T/99aa-like object may contribute substantially to the formation of IME. Brighter 91T/99aa-like SNe may then have more IME than the dimmer ones. Moreover, for 91T/99aa-like objects, pEW_{Si6355} appears to have a stronger correlation with $\Delta m_{15}(B)$ than pEW_{SW} . For example, at -6 d, when $\Delta m_{15}(B)$ increases from 0.8 to 1.0

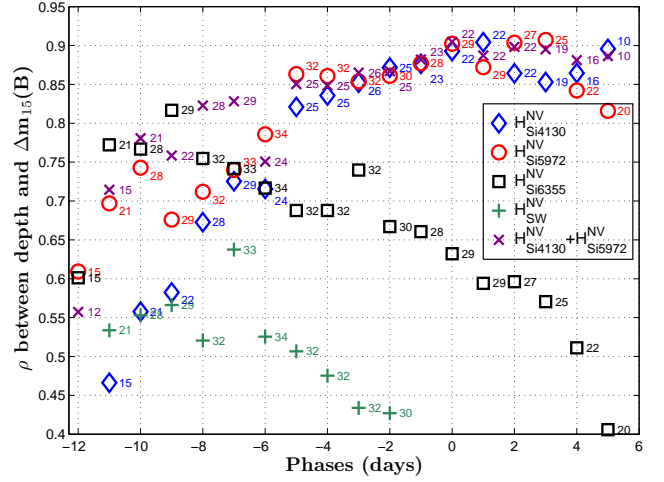


Figure 7. Time-evolutions of the correlations between several indicators and the $\Delta m_{15}(B)$. Superscript “NV” denotes the NV subclass which has a stronger correlation with $\Delta m_{15}(B)$ than other subclasses. Measurements within 2 d were used, and if more than one measurement was available, the one closest to the central phases was used. The sample size is marked on the right for each point.

mag, pEW_{Si6355} decreases from 70 to 10 Å, while pEW_{SW} only decreases from 60 to 30 Å, as shown in the left panels of Figure 8. This may be due to the relatively low abundance of Si II in 91T/99aa-like objects.

Time evolution of the correlation between line strength and $\Delta m_{15}(B)$: As can be seen from Figure 7, the correlations of H_{Si4130} and H_{Si5972} with $\Delta m_{15}(B)$ tend to get stronger from about -10 to about $+2$ d. This may be due to the increase of line strength (meaning more absorptions of the photons and thus a tighter relation with the luminosity), less blending with HVF or neighboring features, and better determination of the pseudo-continuum (see §2). The correlations of H_{Si6355} and H_{SW} with $\Delta m_{15}(B)$, on the contrary, tend to become weaker with time during the same period. The weakening of H_{Si6355} correlation with $\Delta m_{15}(B)$ may be caused by line saturating, as a result of luminosity increase. As one can see from Figure 8, the pEW of Si II $\lambda 6355$ at $t \approx +3$ d barely increases after $\Delta m_{15}(B) = 1.4$ mag. The weakening of H_{SW} correlation with $\Delta m_{15}(B)$ may be due to the decrease of temperature. As shown in the bottom-right panel of Figure 8, at $t \approx +3$ d, pEW_{SW} decreases sharply after $\Delta m_{15}(B) = 1.4$ mag, which could be a sign of too low temperature condition for the highly excited line S II W-trough.

4.3 Velocity differences

The ejecta velocity of SNe Ia varies from object to object, partially due to the asymmetric explosion and line-of-sight effect (Maeda et al. 2010, 2011), and partially due to SN Ia diversity that arises from different progenitor systems and/or explosion mechanisms (see the references given in §1). Even in the same spectrum, different lines still show different velocities, suggesting a layered structure of the SN Ia ejecta (with velocity increasing outward). In this section, we explore the temporal evolution of the velocity differ-

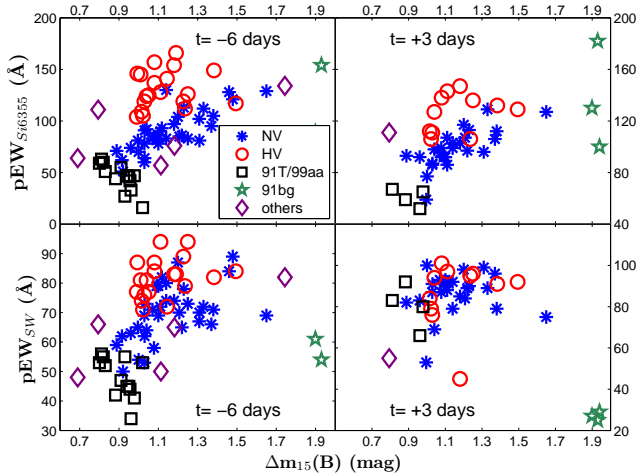


Figure 8. A comparison of the decline-rate dependences of the pEWs of Si II $\lambda 6355$ and S II W-trough at -6 d (left panels) and $+3$ d (right panels). Upper panels: pEWs of Si II $\lambda 6355$ as a function of the decline rate. Lower panels: pEWs of S II W-trough as a function of the decline rate. Measurements within 2 d were used, and if more than one measurement was available, the one closest to the central phases was used. Colors and shapes of data points are the same as in Figure 4.

ences shown between the four spectral features that we study here, and their correlations with $\Delta m_{15}(B)$. Unless otherwise stated, throughout this work a velocity-difference between two features of the same species is defined as the velocity of the longer-wavelength feature minus the velocity of the shorter-wavelength feature.

Deeper layers (corresponding to slower layers) of the ejecta tend to have higher temperatures favoring the occupations of highly-excited states. Therefore, lines from highly-excited states are expected to have lower velocities than lines from lowly-excited states. This is confirmed in Figure 9 which shows rapid increases of the velocity-differences after maximum light, and it could be a sign of accelerating separation between ejecta layers with different thermal condition. The only exception is $V_{S5620} - V_{S5454}$, which remains very small, likely due to that these two lines have very close energy levels (see discussion in §2).

Scatter plots in the upper panels of Figure 10 show details about how $V_{S6355} - V_{SW}$ and $V_{S5972} - V_{S4130}$ are related to $\Delta m_{15}(B)$. The sample is restricted to spectra obtained about 6 d prior to maximum brightness, when the velocities decline linearly with time (see Figure 2). The correlations are overall positive, i.e. fast-decliners tend to have greater $V_{S6355} - V_{SW}$ and $V_{S5972} - V_{S4130}$ than slow-decliners (SN 1991T and SN 1997br appear to be two outliers. In fact, they are also considered as peculiar objects in Hachinger et al. 2006). The direct reason is that V_{SW} and V_{S4130} decrease more rapidly with increasing $\Delta m_{15}(B)$ than V_{S6355} and V_{S5972} (see Figure 5). Physically, this could be explained as that lines with higher excitation and ionization energies are more strongly influenced by the decrease of temperature and luminosity. However, in 91T/99aa-like subclass, $V_{S5972} - V_{S4130}$ appears independent of $\Delta m_{15}(B)$. This is likely due to that these two lines have similar energy levels, and 91T/99aa-like objects have relatively high temperature and luminosity.

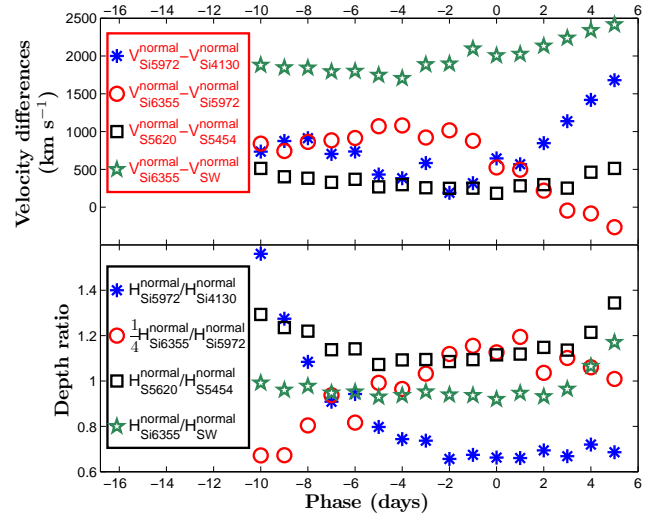


Figure 9. Upper panel: Velocity differences as a function of phase; Lower panel: Depth ratio as a function of phase. The data were averaged over 2 d intervals. Since some 91T/99aa/91bg-like objects have extreme values of velocity difference or depth ratio, here only normal SNe (i.e., NV or HV SNe) are included.

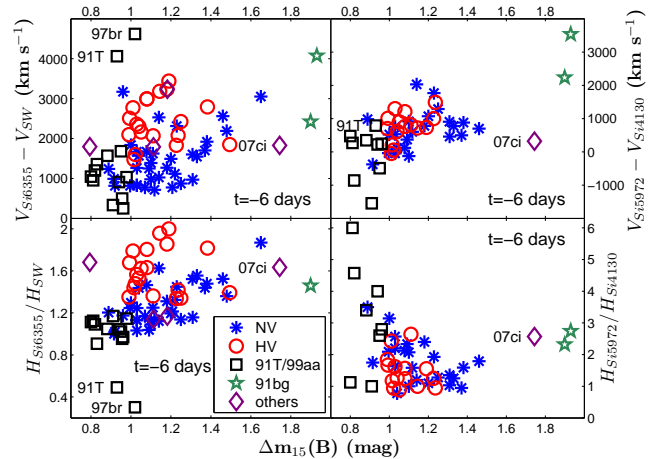


Figure 10. Velocity-differences and depth-ratios versus $\Delta m_{15}(B)$. Measurements within 2 d were used, and if more than one measurement was available, the one closest to the central phases was used. Colors and shapes of data points are the same as in Figure 4.

4.4 Depth ratios

The correlation between the line-strength ratio and $\Delta m_{15}(B)$ has been studied before (e.g., Benetti et al. 2005; Hachinger et al. 2006; Blondin et al. 2012), with the aim to better calibrate SNe Ia as standard candles, or to trace the element abundances in SN Ia ejecta. Most studies focus on correlations at maximum light, and use pEW-ratios to quantify the strength-ratios. However, as mentioned before, the pEW measurement is easily affected by line-blending, and we therefore use the depth-ratio instead. The other reason we use the depth-ratio is that few of this ratio have been explored. Unless otherwise stated, throughout this work a strength-ratio between two features of the same species is

defined as the ratio of the depth of the longer-wavelength feature to the depth of the shorter-wavelength feature.

In Figure 9 we show the time evolution of the depth-ratios. Since some 91T/99aa-like or 91bg-like objects have extreme values of the depth ratios that are not suitable for averaging, this figure includes only normal SNe Ia, i.e. NV or HV groups. It appears that the time evolutions of the depth-ratios share some similarities with the evolutions of the velocity-differences. H_{Si6355}/H_{SW} stays almost unchanged before maximum light (≈ 0.88), suggesting a stable relative-abundance of Si II to S II (see also, Zhao et al. 2015, for a comparison between Si II and Ca II). H_{Si5972}/H_{Si4130} shows the most significant variation with time, possibly due to a competition between these two lines (see discussion in §4.6).

Fast decliners tend to have lower temperatures (except for some peculiar objects, for example, Iax SNe; see, e.g., Foley et al. 2013; Jha 2017), favoring the occupation of lowly-excited states. Therefore, a depth ratio of a longer-wavelength feature to a shorter-wavelength feature (eg., H_{S5620}/H_{S5454}) is expected to increase with increasing $\Delta m_{15}(B)$. This is confirmed in Figure 11, with H_{S5620}/H_{S5454} , H_{Si5972}/H_{Si4130} and H_{Si6355}/H_{SW} showing positive correlations with $\Delta m_{15}(B)$ (as indicated by the positive Pearson coefficients). The only exception is H_{Si6355}/H_{Si5972} , which is anti-correlated with $\Delta m_{15}(B)$, possibly due to high degree of saturation of Si II $\lambda 6355$. Line saturation is quite serious for Si II $\lambda 6355$ which has rather low energy level. At near- or post-maximum epochs, higher luminosity and lower temperature favor for the formation of absorption lines from lowly excited levels. For example, as shown in Figure 12, H_{Si6355} at B -band maximum light ceases to grow after reaching an upper limit of about 0.7 at $\Delta m_{15}(B) \approx 1.4$ mag. While at $t \approx -6$ d, pEW_{Si6355} still persistently grows with $\Delta m_{15}(B)$, as shown in Figure 8.

After maximum light, the correlations between the depth-ratios and $\Delta m_{15}(B)$ decrease quickly with time, as shown in Figure 11. This may be caused by the decreases of temperature and luminosity, and the layers' separations (see discussion in §4.3). H_{Si6355}/H_{SW} also shows a positive correlation with $\Delta m_{15}(B)$, which may be partially due to the fact that dimmer SNe Ia tend to have larger abundance of Si relative to S.

The bottom-left panel of Figure 10 shows details about how the depth ratio H_{Si6355}/H_{SW} (at $t \approx -6$ d) is related to $\Delta m_{15}(B)$. The correlation is overall positive as mentioned above. However, within the 91T/99aa-like subclass, the correlation is reversed, i.e., dimmer objects tend to have smaller H_{Si6355}/H_{SW} . This negative correlation results from H_{Si6355} 's decreasing more rapidly with $\Delta m_{15}(B)$ than H_{SW} in 91T/99aa-like objects, as mentioned in §4.2. The physical reason is unclear. But since temperature and luminosity effects are unlikely the reason, we speculate that brighter 91T/99aa-like objects might have more Si-rich materials than dimmer 91T/99aa-like objects (see discussion in §4.2).

The bottom-right panel of Figure 10 shows a complicated correlation between H_{Si5972}/H_{Si4130} at $t \approx -6$ d and $\Delta m_{15}(B)$. It appears that there is a positive correlation (i.e., dimmer objects have larger H_{Si5972}/H_{Si4130}) for SNe Ia with $\Delta m_{15}(B) > 1.3$ mag, but a negative correlation at $\Delta m_{15}(B) < 1.3$ mag. The positive correlation at $\Delta m_{15}(B) > 1.3$ mag can be explained as that dimmer objects have lower tem-

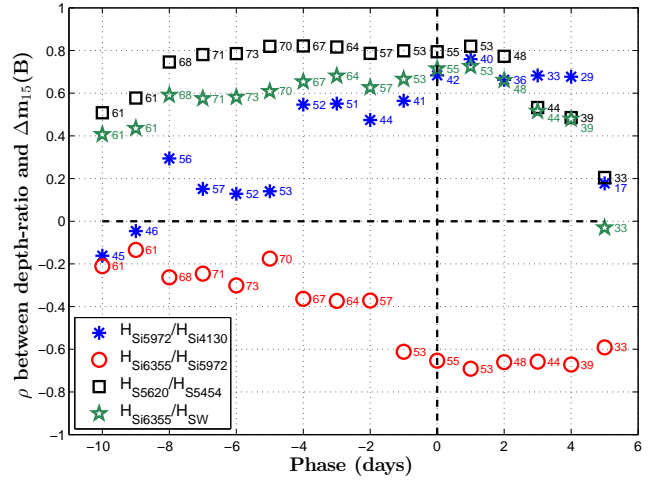


Figure 11. Pearson coefficients between depth (“H”) ratios and the decline rate $\Delta m_{15}(B)$. Measurements within 2 d were used, and if more than one measurement was available, the one closest to the central phases was used. The whole sample, including NV, HV, 91T/99aa-like and 91bg-like SNe are included.

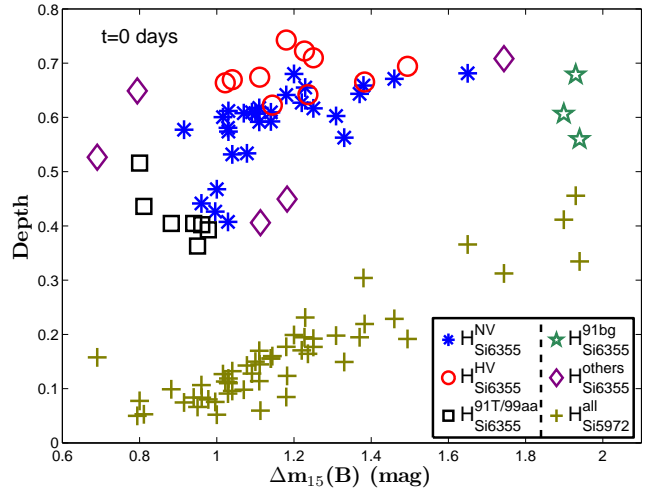


Figure 12. A comparison of the decline-rate dependences of H_{Si6355} and H_{Si5972} . Measurements obtained within 2 d of the maximum light were used, and if more than one measurement was available, the one closest to the specific phase was used.

peratures that would affect Si II $\lambda 4130$ more seriously. It is unclear why the correlation is reversed at $\Delta m_{15}(B) < 1.3$ mag. A possible reason is that brighter objects might have less Si II in the ejecta (as a result of more complete IME burning; see, for example, Benetti et al. 2005), and thus an even smaller chance for the absorption of Si II $\lambda 4130$ (i.e., a more intense competition between Si II features, see the discussion in §4.6).

4.5 Spectroscopic luminosity indicators

Correlations between spectroscopic indicators (velocities, pEWs, pEW-ratios etc.) and photometric parameters ($\Delta m_{15}(B)$, $B - V$ color etc.) have been extensively studied in attempts to improve the accuracy of SN Ia distance

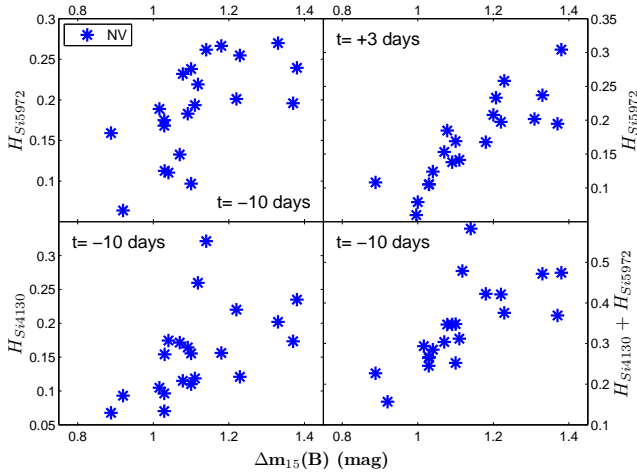


Figure 13. A comparison of the decline-rate dependences of H_{Si4130} (-10 d), H_{Si5972} (-10 and $+3$ d) and $H_{Si4130} + H_{Si5972}$ (-10 d). Measurements within 2 d were used, and if more than one measurement was available, the one closest to the central phases was used. The sample is restricted to normal-velocity (NV) objects only.

measurements (see references given in §1). Using a new sample, we reinvestigate the $\Delta m_{15}(B)$ -dependences of the line strengths of the four lines studied here. Unlike most previous studies, we use the depth to quantify the line strength, instead of the pEW. This is because, as previously mentioned, the depths generally have stronger correlation with $\Delta m_{15}(B)$ than the corresponding pEWs. For example, at $t = -6, -3, 0,$ and $+3$ d, the Pearson correlation coefficient $\rho(pEW_{Si5972}, \Delta m_{15}(B)) = 0.55, 0.71, 0.84,$ and $0.88,$ respectively, while $\rho(H_{Si5972}, \Delta m_{15}(B)) = 0.79, 0.85, 0.90,$ and $0.91,$ respectively. Also, note that measurement of the depth usually has lower uncertainty than that of the pEW. A pEW-measurement usually involves the whole line profile, and consequently it is more subject to line blending and contamination than the depth.

Figure 7 shows several spectroscopic indicators as a function of the $\Delta m_{15}(B)$. The sample is restricted to NV-SNe whose homogeneous spectroscopic properties can help improve the cosmological distance measurements. At early times, $H_{Si5972} + H_{Si4130}$ shows an even stronger correlation with $\Delta m_{15}(B)$ than H_{Si5972} alone, possibly due to an effect of limited element abundance (see §4.6). At maximum light, pEW_{Si5972} shows the strongest correlation with $\Delta m_{15}(B)$, in line with the results of Hachinger et al. (2006) and Blondin et al. (2012). In practice, since it is much easier to obtain a near-maximum spectrum than an early-time spectrum, H_{Si5972} should be more useful than $H_{Si5972} + H_{Si4130}$. H_{Si4130} also has a strong correlation with $\Delta m_{15}(B)$, making it another good indicator of the peak luminosity. And, it is particularly useful for high- z SNe Ia (Nordin et al. 2011), as line Si II $\lambda 4130$ still remains visible in their spectra.

Scatter plots in Figure 13 show more clearly how well H_{Si4130} , H_{Si5972} , and $H_{Si5972} + H_{Si4130}$ correlate with $\Delta m_{15}(B)$. It is clear that at $t \approx -10$ d, $H_{Si5972} + H_{Si4130}$ has the tightest relation with $\Delta m_{15}(B)$. Figure 13 also compares $t \approx -10$ d H_{Si5972} correlation with $\Delta m_{15}(B)$ to that at $t \approx +3$ d. It is clear that the correlation is much tighter at $t \approx +3$ d than at $t \approx -10$ d (see discussions in §4.2).

4.6 Line competition

Since every element has a limited abundance, there could be a competition of two features from the same element. And, the competition could be more intense when these two features have similar energy levels, as they could be closely related in the radiation transport (e.g., Sim et al. 2013; Sim 2017). Below we show some spectral behaviors that could be related to line competition.

As noted in §3.1 and §3.2, Si II $\lambda 5972$ behaves quite differently compared to other features. For example, as shown in Figure 3 (here we focus on NV SNe), during the epoch from -13 to -2 d, Si II $\lambda 5972$ weakens with time, while Si II $\lambda 4130$ strengthens with time. This is hard to explain with temperature effect or abundance difference, as these two features are both from Si II feature and have very similar energy levels. A possible explanation is that Si II $\lambda 5972$ may have serious competition with Si II $\lambda 4130$, forcing the later to be located in a much deeper layers. This also explains the fact that at early times Si II $\lambda 5972$ has a much higher velocity than Si II $\lambda 4130$ (see Figure 2). At maximum light, the competition may be less intense due to relatively high luminosity (and thus more abundant photons), leading to a much smaller velocity difference between Si II $\lambda 5972$ and $\lambda 4130$. Then after maximum light, as the luminosity decreases, the competition may be intensified, causing a rebound of the velocity difference. Similarly, line competition may help explain the great difference between the line strengths of Si II $\lambda 5972$ and $\lambda 4130$. For example, at phases $t \approx -14$ to -10 d, $pEW_{Si4130} \approx \frac{1}{4} pEW_{Si5972}$, while near maximum light, $pEW_{Si4130} \approx pEW_{Si5972}$, as shown in Figure 3. A competition between Si II $\lambda 5972$ and $\lambda 4130$ may also help explain the complicated correlation between strength-ratio H_{Si5972}/H_{Si4130} and $\Delta m_{15}(B)$ (see §10).

A similar case is between the two components of S II W-trough, i.e. S II $\lambda 5454$ and S II $\lambda 5620$, which originate from almost the same levels (E_{lower} : 13.73 eV vs. 13.70 eV, E_{exc} : 2.21 eV vs. 2.27 eV). As shown in Figure 3, before $t \approx -10$ d the redder component has almost twice the strength of the bluer component. While near maximum light, the two components have almost the same strengths. A possible explanation is that there is a competition between the two components. The other possible reason is the saturation effect, as some of the lines from a singly-ionized ion may be saturated for an increasing abundance of the singly-ionized state.

5 CONCLUSIONS

The key to improving the cosmological distance measurements with SNe Ia is to correct for their intrinsic diversity as revealed in the spectral diversity. The aim of this paper is to better understand the physics of the SN Ia features, which would provide a basis for quantitative correction of the intrinsic diversity. We examined four important features of Si II and S II for 554 spectra of 76 SNe Ia, and investigated the time evolutions of their velocities and line strengths, their velocity-differences and depth-ratios, their correlations with $\Delta m_{15}(B)$, and the diversity among the subclasses. Below is a summary of our major findings:

1. *Velocity*: Line velocities generally decrease with time

as expected, but an exception is the velocity of Si II λ 5972, which somehow increases after -2 d and even surpasses the velocity of Si II λ 6355 after $+2$ d. Faster-decliners tend to have faster declining velocities, possibly resulting from faster decrease of temperature.

2. *Line strength*: Before -7 d, line strengths of the two longer-wavelength features, i.e. Si II λ 5972 and 6355 decrease with time, while line strengths of the two shorter-wavelength features, i.e. Si II λ 4130 and S II trough, increase with time. After -7 d, the line strengths of all features increase with time, and reach a flat maxima or plateau near maximum light, except the strength of Si II λ 5972 which reaches a minima near maximum light. A possible reason for the mysterious behavior of Si II λ 5972 might be its competition with other Si II features.

3. *Velocity-pEW correlation*: The overall correlation between velocity and pEW is positive. But for different subclasses at different phases, the correlation can be very different. For example, for HV and 91T/99aa-like objects at -6 d, V_{Si6355} appears to be positively correlated with pEW_{Si6355} . While for NV objects at $+3$ d, V_{Si6355} appears to be anti-correlated with pEW_{Si6355} .

4. $\Delta m_{15}(B)$ -dependence of the velocity: There is an overall trend of increasing velocity for the brighter SNe. But this trend is only significant near $+3$ d, and is almost nonexistent within NV subclass.

5. $\Delta m_{15}(B)$ -dependence of the line strength: Among the NV SNe, there is a trend of stronger Si II and S II features for faster decliners, possibly a result of lower degree of ionization and more remained IMEs in the ejecta of dimmer ones. Among the 91T/99aa-like SNe, on the contrary, slower decliners appear to have stronger Si II and S II absorptions.

6. *Velocity-difference*: There is an overall trend of larger $V_{Si6355} - V_{SW}$ for fainter objects at early times. But within 91T/99aa-like SNe the trend is reversed, possibly due to an effect of ionization. The absolute values of the velocity-differences between different features increase with time after maximum light, suggesting an accelerating separation of the ejecta layers.

7. *Depth-ratio*: Depth-ratios of a longer wavelength feature to a shorter wavelength feature show positive correlations with $\Delta m_{15}(B)$, though the correlations weaken quickly with time after maximum light. The only exception is the H_{Si6355}/H_{Si5972} , which is anti-correlated with $\Delta m_{15}(B)$, possibly due to the saturation of Si II λ 6355. Time-evolutions of the depth-ratios are slower than the evolutions of velocity-differences, especially for H_{Si6355}/H_{SW} , suggesting relatively stable element abundances in the ejecta.

8. *Luminosity indicator*: Less affected by line-blendings, the absorption depths may be better indicators of the luminosity than the corresponding pEWs. Near maximum light, H_{Si5972} shows the strongest correlation with $\Delta m_{15}(B)$, while at early times $H_{Si4130} + H_{Si5972}$ shows the strongest correlation with $\Delta m_{15}(B)$.

The results of this study are very suggestive, but require further investigation. This would require an even larger spectral sample that covers extensive observations of all subtypes. The results of this paper may also help constrain the explosion models (e.g., help determine the abundances of burning products at different phases through the line strengths), or be used to improve the accuracy of SNe Ia as distance indicators. Further theoretical analysis or mod-

eling would be very helpful to better understand the results we obtain here.

ACKNOWLEDGEMENTS

We thank the anonymous referee for his/her insightful suggestions which help improve the paper a lot. The work of X. Wang is supported by National Science Foundation of China (12033003, 11633002, and 11761141001), and the National Program on Key Research and Development Project (grant No. 2016YFA0400803). K.M. acknowledges support provided by Japan Society for the Promotion of Science (JSPS) through KAKENHI grant (17H02864, 18H04585, 18H05223, 20H00174, and 20H04737). This research has made use of the CfA Supernova Archive, which is funded in part by the US National Science Foundation through grant AST 0907903. This research has also made use of Berkeley/Lick Supernova Archives, which is funded in part by the US National Science Foundation. This research has also made use of the CSP Supernova Archive, which is supported by the World Premier International Research Center Initiative (WPI).

DATA AVAILABILITY

The authors confirm that the data supporting the findings of this study are available within the article and its supplementary materials.

REFERENCES

- Altavilla, G. et al., 2007, A&A, 475, 585
 Anderson, J. P. et al., 2015, MNRAS, 448, 732
 Bailey, S. et al., 2009, A&A, 500, L17
 Benetti, S. et al., 2005, ApJ, 623,1011
 Betoule, M. et al., 2014, A&A, 568, A22
 Blondin, S., Mandel, K. S., Kirshner, R. P., 2011, A&A, 526,81
 Blondin, S. et al., 2012, AJ143, 126
 Blondin, S., Dessart, L., Hillier, D. J. & Khokhlov, A. M., 2017, MNRAS, 470, 157
 Branch, D. et al., 2006, PASP, 118, 560
 Brown, P. J., Perry, J. M., Beeny, B. A., Milne, P. A., Wang, X., 2018, ApJ, 867, 56
 Brown, P. J., Hosseinzadeh, G., Jha, S. W., Sand, D., Xiang, D., 2019, ApJ, 877, 152
 Brown, P. J. Crumpler, N. R., 2020, ApJ, 890, 45
 Bulla, M. et al., 2016, MNRAS, 462, 1039
 Burns, C. R. et al, 2014, ApJ, 789, 32
 Cao, Y. et al., 2015, Nature, 521, 328
 Childress, M. J. et al., 2013, ApJ, 770, 29
 Childress, M. J., Filippenko, A. V., Ganeshalingam, M., Schmidt, B. P., 2014, MNRAS, 437, 338
 Churazov, E. et al., 2014, Nature, 512, 406
 Cleveland, W. S., 1979, Journal of the American Statistical Association, 74, 368
 Dhawan S., Jha S. W., Leibundgut B., 2018, A&A, 609, 72
 Dilday, B. et al., 2012, Science, 337, 942
 Ellis, R. S. et al., 2008, ApJ, 674, 51
 Filippenko, A. V. et al., 1992a, AJ, 104, 1543
 Filippenko, A. V. et al., 1992b, ApJ, 384, L15
 Filippenko, A. V., 1997, ARA&A, 35, 309
 Fink, M., Röpke, F. K., Hillebrandt, W., Seitenzahl, I. R., Sim, S. A., Kromer, M., 2010, A&A, 514, 53

- Fisher A., Branch D., Hatano K., Baron E., 1999, *MNRAS*, 304, 67
- Flörs, A. et al., 2020, *MNRAS*, 491, 2902
- Folatelli, G. et al., 2012, *ApJ*, 745, 74
- Folatelli, G. et al., 2013, *ApJ*, 773, 53
- Foley, R. J., Kasen, D., 2011, *ApJ*, 729, 55
- Foley, R. J., Sanders, N. E., Kirshner, R. P., 2011, *ApJ*, 742, 89
- Foley, R. J. et al., 2013, *ApJ*, 767, 57
- Foley, R. J. et al., 2020, *MNRAS*, 491, 5991
- Friedman, A. S. et al., 2015, *ApJS*, 220, 9
- Freedman, W. L. et al., 2019, *ApJ*, 882, 34
- Ganeshalingam, M. et al., 2010, *ApJS*, 190, 418
- Ganeshalingam, M., Li, W., Filippenko, A. V. 2011, *MNRAS*, 416, 2607
- Garavini, G. et al., 2007, *A&A*, 471, 527
- Garnavich, P. M. et al., 2004, *ApJ*, 613, 1120
- Guillochon, J., Parrent J., Kelley L. Z., Margutti R., 2017, *ApJ*, 835, 64
- Hachinger, S., Mazzali, P. A., Benetti, S., 2006, *MNRAS*, 370, 299
- Hachinger, S., Mazzali, P.A., Tanaka, M., Hillebrandt, W., Benetti, S., 2008, *MNRAS*, 389, 1087
- Hachinger S., Mazzali P.A., Taubenberger S., Pakmor R., Hillebrandt W., 2009, *MNRAS*, 399, 1238
- Hamuy, M. et al., 2003, *Nature*, 424, 651
- Hatano, K., Branch, D., Fisher, A., Baron, E., Filippenko, A. V., 1999, *ApJ*, 525, 881
- Hatano, K. et al., 2000, *ApJ*, 543, L49
- Hill, R. et al., 2018, *MNRAS*, 481, 2766
- Hillebrandt, W., Niemeyer, J. C., 2000, *ARA&A*, 38, 191
- Hoeflich, P. et al., 1996, *ApJ*, 472, L81
- Howell, D. A., Höflich, P., Wang, L., Wheeler, J. C., 2001, *ApJ*, 556, 302
- Howell, D. A. et al., 2009, *ApJ*, 691, 661
- Hsiao, E. Y. et al., 2015, *A&A*, 578, 9
- Iben, I., Tutukov, A. V., 1984, *ApJS*, 54, 355
- Jacobson-Galán, W. V. et al., 2019, *MNRAS*, 487, 2538
- Jha, S. et al., 2006, *AJ*, 131, 527
- Jha, S. W., 2017, in *Handbook of Supernovae*, ed. A. W. Alsabti & P. Murdin (Cham: Springer International Publishing), 375
- Jha, S. W., Maguire, K., Sullivan, M., 2019, *Nature Astronomy*, 3, 706
- Jones, D. O., Scolnic, D. M., Riess, A. G., 2018, *ApJ*, 857, 51
- Kasen, D. Woosley, S. E., 2007, *ApJ*, 656, 661
- Kawabata, M. et al., 2020, *ApJ*, 893, 143
- Kato, M., Saio, H., Hachisu, I., 2018, *ApJ*, 863, 125
- Kerzendorf, W. E., Childress, M., Scharwächter, J., Do, T., Schmidt, B. P., 2014, *ApJ*, 782, 27
- Khokhlov, A. M., 1991, *A&A*, 245, 114
- Li, W. D. et al., 2001, *ApJ*, 546, 734
- Li, W. D. et al., 2003, *PASP*, 115, 453
- Li, W. D. et al., 2011, *Nature*, 480, 348
- Li, W. X. et al., 2020, arXiv:2011.07240
- Liu, D., Wang, B. Han, Z., 2018, *MNRAS*, 473, 5352
- Livio, M. Mazzali, P., 2018, *Physics Reports*, 736, 1
- Maeda, K. et al., 2010, *Nature*, 466, 82
- Maeda, K., Leloudas, G., Taubenberger, S., Stritzinger, M., Sollerman, J., 2011, *MNRAS*, 413, 3075
- Maeda, K., Terada, Y., 2016, *Int. J. Mod. Phys. D*, 25, 1630024
- Maeda, K., Jiang, J., Shigeyama, T., Doi, M., 2018, *ApJ*, 861, 78
- Maguire, K. et al., 2012, *MNRAS*, 426, 2359
- Maguire, K. et al., 2013, *MNRAS*, 436, 222
- Maguire, K. et al., 2014, *MNRAS*, 444, 3258
- Maguire, K. et al., 2018, *MNRAS*, 477, 3567
- Mandel, K. S., Foley, R. J., Kirshner, R. P., 2014, *ApJ*, 797, 75
- Mandel, K. S., Scolnic, D. M., Shariff, H. et al., 2017, *ApJ*, 842, 93
- Maoz D., Mannucci F., Nelemans G., 2014, *ARA&A*, 52, 107
- Marion, G. H. et al., 2015, *ApJ*, 798, 39
- Matheson, T. et al., 2008, *AJ*, 135, 1598
- Mazzali P. A., Danziger I. J., Turatto M., 1995, *A&A*, 297, 509
- Mazzali, P. A., Chugai, N., Turatto, M. et al., 1997, *MNRAS*, 284, 151
- Mazzali, P. A., Nomoto, K., Cappellaro, E. et al., 2001, *ApJ*, 547, 988
- Mazzali, P. A. et al., 2005a, *MNRAS*, 357, 200
- Mazzali, P. A. et al., 2005b, *ApJ*, 623, L37
- Mazzali, P. A. et al., 2014, *MNRAS*, 439, 1959
- Meng, X., 2019, *ApJ*, 886, 58
- Mulligan, B. W., Wheeler, J. C., 2017, *MNRAS*, 467, 778
- Mulligan, B. W. Zhang, K. & Wheeler, J. C., 2019, *MNRAS*, 484, 4785
- Nomoto, K., 1982, *ApJ*, 253, 798
- Nomoto, K., Thielemann, F. K., Yokoi, K. 1984, *ApJ*, 286, 644
- Nomoto K., Iwamoto K., Kishimoto N., 1997, *Science*, 276, 1378
- Nomoto, K., Kamiya, Y., Nakasato, N., 2013, *IAU Symposium*, 281, 253
- Nomoto, K., Leung, S., 2018, *Space Science Reviews*, 214, 67
- Nordin, J. et al., 2011, *ApJ*, 734, 42
- Nugent, P., Phillips, M., Baron, E., Branch, D., Hauschildt, P., 1995, *ApJ*, 455, L147
- Olling, R. P. et al., 2015, *Nature*, 521, 332
- Parrent, J. T. et al., 2011, *ApJ*, 732, 30
- Parrent, J., Friesen, B., Parthasarathy, M., 2014, *Ap&SS*, 351, 1
- Patat, F. et al., 1996, *MNRAS*, 278, 111
- Patat, F., Benetti, S., Cappellaro, E., Turatto, M., 2006, *MNRAS*, 369, 1949
- Patat, F. et al., 2007, *Science*, 317, 924
- Pereira R. et al., 2013, *A&A*, 554, 27
- Perlmutter, S. et al., 1999, *ApJ*, 517, 565
- Phillips, M. M., 1993, *ApJ*, 413, L105
- Phillips, M. M. et al., 1992, *AJ*, 103, 1632
- Phillips, M. M. et al., 1999, *AJ*, 118, 1766
- Pignata, G. et al., 2004, *MNRAS*, 355, 178
- Riess, A. G. et al., 1998, *AJ*, 116, 1009
- Riess A. G. et al., 2016, *ApJ*, 826, 56
- Riess A. G., Casertano S., Yuan W., Macri L. M. Scolnic D., 2019, *ApJ*, 876, 85
- Ruiter, A. J. et al., 2013, *MNRAS*, 429, 1425
- Sasdelli, M., Mazzali, P.A., Pian, E., Nomoto, K., Hachinger, S., Cappellaro, E., Benetti, S., 2014, *MNRAS*, 445, 711
- Schaefer, B. E., Pagnotta, A., 2012, *Nature*, 481, 164
- Scolnic, D. M. et al., 2018, *ApJ*, 859, 101
- Shen, K. J., Bildsten, L., 2014, *ApJ*, 785, 61
- Silverman, J. M. et al., 2012a, *MNRAS*, 425, 1789
- Silverman, J. M. et al., 2012b, *MNRAS*, 425, 1819
- Silverman, J. M., Ganeshalingam, M., Li, W., Filippenko, A. V., 2012c, *MNRAS*, 425, 1889
- Silverman, J. M. et al., 2012d, *MNRAS*, 425, 1917
- Silverman, J. M. et al., 2015, *MNRAS*, 451, 1973
- Sim, S. A. et al., 2012, *MNRAS*, 420, 3003
- Sim, S. A. et al., 2013, *MNRAS*, 436, 333
- Sim, S. A., 2017, in *Handbook of Supernovae*, ed. A. W. Alsabti & P. Murdin (Cham: Springer International Publishing), 769.
- Stahl, B. E. et al., 2020, *MNRAS*, 492, 4325
- Sternberg, A. et al., 2011, *Science*, 333, 856
- Stritzinger, M. D., Phillips, M. M. et al., 2011, *AJ*, 142, 156
- Tanaka, M. et al., 2008, *ApJ*, 677, 448
- Taubenberger, S., in *Handbook of Supernovae*, ed. A. W. Alsabti & P. Murdin (Cham: Springer International Publishing), 317
- Thomas, R. C., Aldering, G., Antilogus, P. et al., 2011, *ApJ*, 743, 27
- Wang, X., Filippenko, A. V., Ganeshalingam, M. et al., 2009, *ApJ*, 699, L139
- Wang, X., Wang, L., Filippenko, A. V., Zhang, T., Zhao, X., 2013, *Science*, 340, 170

- Wang, X., Chen, J., Wang, L., Hu, M., Li, W., 2019, ApJ, 882, 120
- Webbink, R. F., 1984, ApJ, 277, 355
- Whelan, J., Iben, I., 1973, ApJ, 186,1007
- Wilk, K. D., Hillier, D. J., Dessart, L., 2018, MNRAS, 474, 3187
- Wu, C., Wang, B., Wang, X., Maeda, K., Mazzali, P., 2020, MNRAS, 495, 1445
- Zhang, T. et al., 2010, PASP, 122, 1
- Zhang, T. et al., 2015, Research in Astronomy and Astrophysics, 15, 215
- Zhang, J. et al., 2015, ATel, 7109
- Zhao, X. et al., 2015, ApJS, 220, 20
- Zhao, X. et al., 2016, ApJ, 826, 211
- Zheng, W. et al., 2013, ApJ, 778, L15
- Zheng, W. et al., 2017, ApJ, 841, 64

This paper has been typeset from a $\text{\TeX}/\text{\LaTeX}$ file prepared by the author.